

Exploration of High Efficiency AIE-Active Deep/Near-Infrared Red Emitters in OLEDs with High-Radiance

Qing Wan, Jialin Tong, Bing Zhang, Yin Li, Zhiming Wang,* and Ben Zhong Tang*

Limiting by classic donor–acceptor (D–A) strategy based on charge transfer (CT) process dominated emission, the high-efficiency organic deep/near infrared red (DR/NIR) emitters with desirable photoluminescence quantum yields (PLQYs) and satisfactory excitons utilization efficiencies (EUEs) are still a challenge. Herein, three new DR/NIR luminogens (TNZPPI, TNZtPPI and TNZ2tPPI) based on naphtho[2,3-c][1,2,5]thiadiazole (NZ) group are synthesized. Their interesting characterization of hybrid excited states containing tuned local excited (LE) and CT components are confirmed, and the effective high-lying reverse intersystem crossing (RISC) channel might be activated because of their larger T_2 – T_1 energy gap and smaller T_4 – S_2 energy splitting. Thanks for their higher fluorescence quantum yields in film (24–38%), the TNZPs-based non-doped devices exhibit bright NIR emission with higher maximum radiance of 21447–36027 mW Sr^{−1} m^{−2}, whose performance are better than most reported pure organic NIR devices. Enjoying deep analysis of their solvation effect and aggregation-induced emission (AIE)-activity, the doped organic light emitting diodes (OLEDs) are fabricated, whose performances are very good with identical National Television System Committee saturated red-emitting behaviors. The results in TNZPs show that the electronic effect of molecule structure and intermolecular interactions all are relative to their performance, and which is very important for the design high-efficiency NZ-based OLED materials.


1. Introduction

In the past decades, organic light emitting diodes (OLEDs) have achieved great success in flat-panel displays because of their advantages of high-quality resolution, low cost, light weight, and flexibility.^[1–5] However, the development of new generation displays urges to extend the spectrum of OLEDs from visible to deep/near-infrared red (DR/NIR, $\lambda_{\text{EL}} \geq 650$ nm) owing to their potential applications in optical communication, information-secured displays, night-vision devices, and sensors.^[6–8] Similar to most OLEDs' luminescent materials, the photoluminescence quantum yield (PLQY) in solid state and exciton utilization efficiency (EUE) in DR/NIR emitters are two main factors for achieve high electroluminescence (EL) efficiencies.^[9,10] While in the classic donor–acceptor (D–A) strategy based on charge transfer (CT)-dominated emission, the DR/NIR luminescence efficiency usually become very low, and their excitons tend to be wasted in nonradiative transition channel.^[11]

Recently, a new building block named naphtho[2,3-c][1,2,5]thiadiazole (NZ) as electronic acceptor has attracted more and more attention in constructing DR/NIR emitters by coupling with different donors on its both sides. Integrating with its derivatives' photophysical behaviors, OLEDs performance, and theoretical calculation, the hybrid localized and charge transfer (HLCT) mechanism plays an important role in their electroluminescence process, and the efficient upper reverse intersystem crossing (uRISC) activation from triplet excitons to singlet ones has improved their internal quantum efficiency (IQE) and the radiative transition proportion.^[9,12–15] For example, Yang group had realized 3.9% of external quantum efficiency (EQE) in nondoped devices via optimizing symmetrical derivatives as emitters,^[16] and Ma group fabricated two unsymmetrical emitters to achieve better performance with desirable internal quantum efficiency (IQE \approx 100%).^[17] Contrary to common NZ-based sandwich structures connecting two donors, Ma and co-workers also inserted an acceptor to one side, and the high-efficiency NIR devices with enhanced fluorescent efficiency and EUE were observed.^[18] Regrettably, most of the substituted groups have some spatial hindrance, which would be benefit to inhibit the stronger intermolecular packing interaction for improving luminous efficiency in solid

Dr. Q. Wan, Dr. B. Zhang, Dr. Y. Li, Prof. Z. Wang, Prof. B. Z. Tang
Center for Aggregation-Induced Emission
Key Laboratory of Luminescence from Molecular Aggregates of
Guangdong Province
State Key Laboratory of Luminescent Materials and Devices
South China University of Technology
Guangzhou 510640, China
E-mail: wangzhiming@scut.edu.cn; tangbenz@ust.hk

Dr. J. Tong
School of Petrochemical Engineering
Shenyang University of Technology
Liaoyang 111003, China
Prof. B. Z. Tang
Department of Chemistry
Hong Kong Branch of Chinese National Engineering Research Center
for Tissue Restoration and Reconstruction
Institute for Advanced Study
and Department of Chemical and Biological Engineering
The Hong Kong University of Science and Technology
Clear Water Bay, Kowloon, 999077 Hong Kong, China

 The ORCID identification number(s) for the author(s) of this article can be found under <https://doi.org/10.1002/adom.201901520>.

DOI: 10.1002/adom.201901520

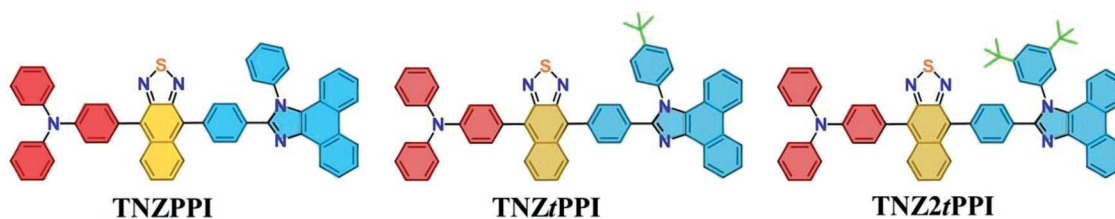


Figure 1. Chemical structure of TNZPPI, TNZtPPI, and TNZ2tPPI.

but is not ideal for carriers transporting process in OLED operation.

Herein, we would introduce 1,2-diphenyl-1H-phenanthro[9,10-d]-imidazole (PPI) unit as a large planar substitution group with bipolar characteristic to triphenylamine (TPA)-modified NZ derivative (TNZ) for enhancing carriers injecting/transporting capability, and TNZPPI was prepared firstly as shown in **Figure 1**, where, the PPI group would also increase brightness according to our previous report.^[19] To demonstrate the importance of this planar group, the tert-butyl group with different steric effect group was inserted to modify PPI, which would inhibit intermolecular stacking interaction between phenanthrene-based planes, and TNZtPPI and TNZ2tPPI were synthesized as two models. Combining with systematic spectral experiment and theoretical calculation of the three NZ-based new emitters (TNZPPI, TNZtPPI, and TNZ2tPPI), their unique HLCT feature and aggregation-induced emission (AIE) activity were observed, and the difference of their excited state component dependent on environmental polarity change were discussed in details. Luckily, TNZPPI and TNZ2tPPI all exhibited higher luminescence efficiency (>30%) in film than common NZ-based materials. Thanks for “hot exciton” channel activated in the EL process and effective carriers transport process after inserting PPI plane, the nondoped OLED device of TNZPPI achieved higher device efficiency of 2.48% with greater radiance efficiency of 36 027 mW Sr⁻¹ m⁻² at electroluminescence (EL) of 686 nm, significantly better than its tert-butyl derivatives and most reported NZ-based materials. In doped devices, their Commission Internationale de L'Eclairage (CIE) of EL emission had reached the requirement of standard saturated red light (SSRL) devices with CIE of (0.67, 0.33) defined by the National Television System Committee (NTSC). The EQE of SSRL device was achieved at 6.83% when the doped 10 wt% TNZPPI in the CBP host, which is the highest efficiency of SSRL devices at present. All results show that, it is a good strategy to insert multifunctional plane substitutes for tuning NZ-based DR/NIR emitters, especially in improving OLEDs' performance.

2. Results and Discussion

2.1. Synthesis and Characterization

Similar to most of NZ-based compounds, the targeted molecules of TNZPPI, TNZtPPI, and TNZ2tPPI (uniformly named as TNZPs) were synthesized by multistep coupling reaction as shown in Figure S1 (Supporting Information). First, the core intermediate product of NZ unit was prepared via the

cyclization reaction between 2,3-diaminonaphthalene and *N*-thionylaniline with a better yield of 77%,^[14] and the subsequent bromination procedure (DBr-NZ) was operated using liquid bromine as Br-donating moiety with an optimized yield of 64%. After then, the commercial TPA-based boronic acid was introduced to connect with DBr-NZ, and the monosubstituted intermediate of TNZ-Br was obtained via classical palladium-catalyzed Suzuki reaction. Alternately, three PPI-Br derivatives were prepared via tuning structures of corresponding aromatic amines (aniline, 4-tert-butylaniline, and 3,5-di-tert-butylaniline) as our previous reports, and their borate esterification (PPI-B) process were done with yields of 58–74% according to the literatures with slight modification.^[20,21] Employing the Suzuki reaction again, three TNZPs were obtained, and purified by column chromatography, whose structures were confirmed by spectroscopical characterization using nuclear magnetic resonance spectroscopy (Figures S21–S26, Supporting Information) and high-resolution mass spectrometry (Figures S2–S4, Supporting Information).

2.2. Theoretical Simulation and Calculation

In order to discuss the effect of the introduction of TPA and PPI groups on the ground and excited states of NZ-based derivatives and the difference between three of them originated from tert-butyl groups modification, the density functional theory (DFT) and time-dependent DFT (TD-DFT) calculation were carried out by the M06-2X/6-31g(d,p) level.

The optimized geometries of TNZPs at ground state in the gas phase was shown in **Figure 2**, and their similar dihedral angles were observed at about 52° between the NZ group and its adjacent phenyl ring in TPA unit, but the other twisted angles between the NZ and another adjacent phenyl group of PPIs were increased from 53.7° to 56° due to the insert of tert-butyl segment with different pattern. Combining the propeller conformation of TPA, three TNZPs displayed comparative distorted conformation, which could inhibit stronger intermolecular interaction to some extent.^[22] Interestingly, the dihedral angles between the phenyl group containing tert-butyl group at N1 substitution of PPI and the plane of phenanthrene derivatives displayed relatively irregular change. Comparing to TNZPPI, this dihedral angle of TNZtPPI gave a little increment, because of their similar substituent framework between phenyl and *p*-tert-butyl phenyl group. While, the dihedral angle in TNZ2tPPI became smaller, it might be contributed to the interaction between hydrogen atoms in *m*-tert-butyl group and heteroatoms in NZ unit. Even so, the effect of introducing large steric effect group to inhibit intermolecular interactions from PPI unit had

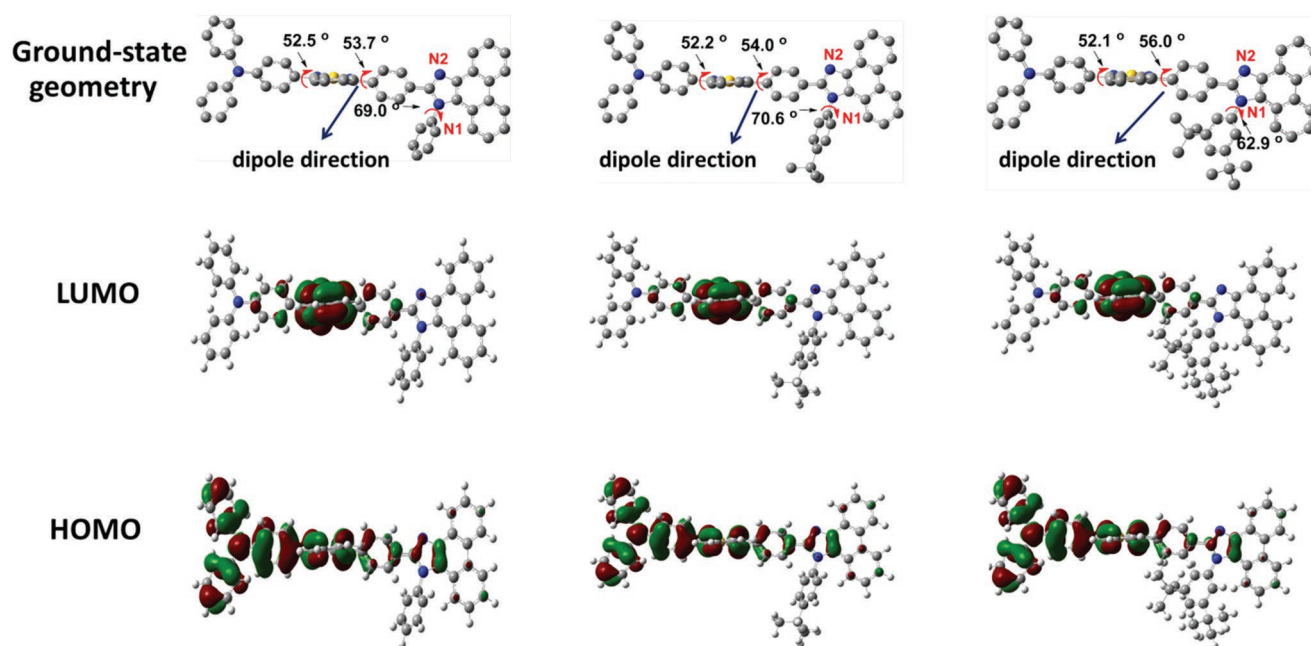


Figure 2. Optimized geometry and HOMO/LUMO distributions of TNZPPI, TNZtPPI, and TNZ2tPPI in ground states. Blue arrow: the direction of dipole moment at ground state (simulated by M062X/6-31g(d,p) level using Gaussian 09 package).

been speculated as shown in Figure S5 (Supporting Information). The distance between the parallel plane containing H in N1-substitutive phenyl group and PPI plane was about 1.86 Å, and was increased to 2.16 Å after inserting *p*-tert-butyl phenyl group. And the value became 4.21 Å when two *m*-tert-butyl segments inserted, which would effectively inhibit intermolecular stacking interaction, usually having positive effect on enhancing the fluorescence efficiency in aggregates.

To their electron distribution of the highest occupied molecular orbital (HOMO) and lowest unoccupied molecular orbital (LUMO) at ground state, there was little difference. The HOMOs all mainly dispersed at TPA and NZ group with some in phenyl and imidazole group of PIMs, implying TPA group might play a key role in asymmetric electron-donating substituents than PPI (weak donor in our previous reports).^[20,23] The LUMOs located at NZ group with a little at two adjacent phenyl groups, and there was no significant effect on the electron distribution region after the introduction of tert-butyl group. Usually, this distribution of the HOMO and LUMO partially overlap was usually beneficial of enhancing PLQYs, at least in low-polar solvents (such as hexane). However, their ground state dipole moments increased from 4.54 D for TNZPPI, to 4.93 D for TNZtPPI, to 4.95 D for TNZ2tPPI, respectively. If the NZ and PPI with different substituted groups were considered as a composite electron acceptor, their electron-withdrawing ability increased gradually, indicating the tert-butyl substituted compounds might have stronger intramolecular charge transfer (ICT) effect, which was unfavorable to luminous efficiency improvement at unimolecular level, and the conjecture would be confirmed by the subsequent solvatochromism effect.

In the previous NZ-based work,^[3,16] NZ had been regarded as the key block to achieve high excitons utilization efficiencies (EUEs), showing good RISC capability via HLCT mechanism.

Herein, the natural transition orbitals (NTOs) of S_1 – S_5 and T_1 – T_5 orbitals of three TNZPs were further carried out based on TD-DFT at the M06-2X/6-31G(d,p) level for obtaining insight into the relationship between the structure and orbitals distribution (Figures S6–S8, Supporting Information). Three TNZPs possessed similar electron structure at S_1 state. The particles were centralized on the acceptor NZ unit, and the holes were dispersed on the TPA–NZ and adjacent phenyl ring, suggesting the coexistence of LE and CT components at S_1 state. Unlike common DR emitters via enhancing D–A effect to increase the emission peak location, this hybridization local excited (LE) composition in their excited states increased significantly, which was crucial for improving the luminescence efficiency than CT-dominant emitters. After then, the energy levels of the first five singlet and triplet states were further calculated (Figure S9, Supporting Information). Taking TNZPPI as an example, the large energy splitting between S_1 (2.62 eV) and T_1 (1.46 eV) was calculated as 1.16 eV (Figure 3), which could demonstrate unfavorable RISC process of $T_1 \rightarrow S_1$, and the potential thermal active delay fluorescence (TADF) process would become very difficult according to this value. As expected, a large energy gap (1.53 eV) between T_2 (2.99 eV) and T_1 (1.46 eV) state was observed, which would be benefit to suppress internal conversion (IC) process from T_2 to T_1 .^[24] At the same time, the small energy difference ($\Delta E_{st} = 0.08$ – 0.27 eV) between T_{4-2} and S_2 were shown, which could effectively facilitate the triplet excitons to singlet ones conversion channel by uRISC process via suppressing the $T_2 \rightarrow T_1$ IC process according energy gap law. In addition, the high-lying levels of T_2 , T_3 , and T_4 displayed LE-dominant hybridization composition or LE state, and the S_2 showed CT-dominant HLCT hybrid state. Nevertheless, the coexistence of LE and CT states in the S_2 and T_{4-2} states was also benefited to the uRISC process according to the

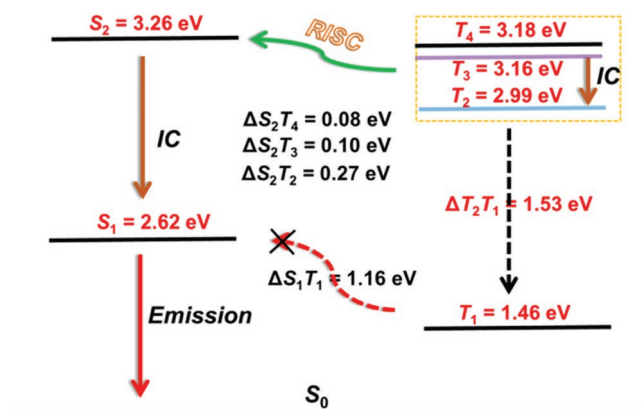


Figure 3. The energy level and calculated HOMO/LUMO spatial distribution of TNZPPI.

permissible spin-orbit coupling (SOC) between the singlet and the triplet states.^[25–27] Therefore, these three factors (upper singlet-triplet excitons with permissible SOC characters, large T_2T_1 energy gap and smaller energy barriers) would generally enhance NZ-based molecules to enjoy good EUEs. The others (TNZ*t*PPI and TNZ2*t*PPI) possessed similar NTOs and energy level distribution. Consequently, we believed that three asymmetric substituted NZ-derivatives should be beneficial for high luminescence efficiency and suitable exciton conversion channels, well matched with the “hot excitons” channel principle, which was necessary for high-performance OLED emitters.

2.3. Photophysical Property

Based on the theoretical analysis of single molecule level above, some systematic spectral experiments were carried out in solution for discussing the ground- and excited-state optical properties of TNZPs. Although three TNZPs enjoyed more aromatic structures in the framework, they had good solubility in common organic solvents, such as hexane, tetrahydrofuran, and dimethyl formamide (DMF) at the concentration of about 10^{-5} M, but poor solubility in water. As shown in Figure S10 (Supporting Information), the same two main absorption bands in DMF were observed for three TNZPs. Herein, the first one located at 311 nm was contributed to the $\pi \rightarrow \pi^*$ transition of conjugated aromatic skeleton, and the weaker one extends to 506 nm should be from ICT state due to their D–A structure as the above theoretical calculations described. To their PL spectra, the TNZPs luminogens in DMF exhibited DR/NIR fluorescence with maximal emission peaks of 662 nm for TNZPPI, 686 nm for TNZ*t*PPI, and 685 nm for TNZ2*t*PPI, respectively. There was obvious 20 nm red-shift after inserting tert-butyl group, implying some difference existed in their excited state of TNZ*t*PPI and TNZ2*t*PPI than TNZPPI.

For comparing details of ground/excited-state properties along with the environmental polarity change, their absorption and PL measurements of three chromophores in various solvents were collected (Figures S11 and S12, Supporting Information). At the same time, their PLQYs and lifetime in different

polar solvents were investigated, too (Tables S1–S3, Supporting Information). Accompany with the increase of environmental polarity, their absorption bands showed a little shift, implying the ground state was insensitive to solvent polarity. While to their excited-state properties, the obvious red-shift emission along with the decreased PLQYs was observed, indicating their excited-state was very sensitive to polar environment. Taking TNZPPI as an example, its emission peak location was shifted from 621 nm in low-polarity hexane to 662 nm in high-polarity DMF, and the 41 nm solvatochromic shift was given. While in the others, the shifts were extended to 67 nm for TNZ*t*PPI and 66 nm for TNZ2*t*PPI, respectively. Generally, this red-shift caused by solvent polarity change was originated from the CT component increase in their respective lowest excited state, for LE component was unaffected by solvents according to HLCT theory.^[9] To three TNZPs with similar framework, their LE state constitution seemed the same, and their obvious difference should be from the interaction intensity between donor (TPA) and acceptor (NZ+PPI) caused by the steric effect of tert-butyl group instruction. Therefore, the redundant 25/24 nm red-shifted from TNZPPI to TNZ*t*PPI/TNZ2*t*PPI demonstrated that the proportion of CT state increased faster in S_1 after the introduction of tert-butyl group along with environmental polarity increasing, which was consistent with previous theoretical predication of their excited state dipole.

To clearly demonstrate the change above, the Lippert–Mataga model was used to evaluate the dipole moment (μ_e) of excited state by comparing slope of the stoke shift ($\nu_a - \nu_f$) versus the polarity of organic solvents (f).^[28] Where, the excited state μ_e was smaller and near to 10 D, and the LE state was dominant component to S_1 . If μ_e was larger than the typical CT molecule DMABN of 23 D,^[29] the CT state was dominant component. Between the both, the mixed state was considered as a hybridized composition containing LE and CT component. As shown in Figure 4, three TNZPs all displayed nonlinearity assigned to two different linear correlation in low-polarity and high-polarity solvents. In low-polarity solvent, they had similar and smaller straight-line slopes of 10.79 D for TNZPPI, 10.80 D for TNZ*t*PPI, and 10.32 D for TNZ2*t*PPI, respectively, implying they did have similar LE state. While in high-polarity solvent, the fitted line yields their large slopes of 11.62 D for TNZPPI, 15.32 D for TNZ*t*PPI, and 18.60 D for TNZ2*t*PPI, respectively, demonstrating the CT component was enhanced at their respective excited state, where TNZ*t*PPI and TNZ2*t*PPI were more sensitive to the environmental polarity than TNZPPI due to the effect of tert-butyl group insert, which was consistent to our speculation from calculation. Meanwhile, three DR emitters' efficiencies gave a significant decrease trend, and their PLQYs were decreased from about 80% in hexane to 3% in DMF, which was coincided with the increase of CT states above. In addition, the transient fluorescence and photoluminescence decay spectra of TNZPs were measured, and they all exhibited short fluorescent lifetime as shown in Figure S13 (Supporting Information), which could also eliminate the TADF possibility. Respectively, according to the low-temperature fluorescence and phosphorescence spectra at 77 K (Figure S14, Supporting Information), their low-temperature fluorescence peaks were closed to the room-temperature emission position, but the low-temperature phosphorescent signal was difficult to be detected,

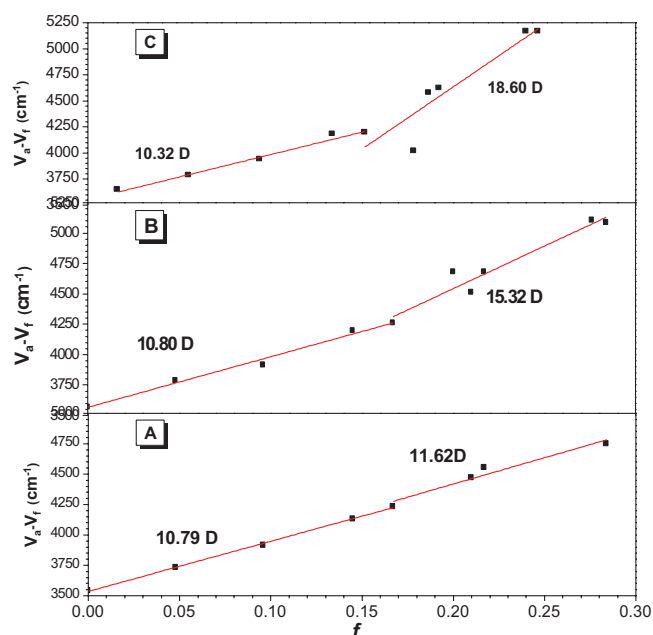


Figure 4. Linear correlation of polarity of solvent media with Stoke shift ($\nu_a - \nu_f$) for A) TNZPPI, B) TNZtPPI, and C) TNZ2tPPI.

demonstrating that the low-lying T_1 state was not easy to form by the IC process via photoexcitation or difficult detect in routine measurement.

The luminescence behaviors of three DR emitters in aggregates were further discussed. In neat film via vacuum evaporation preparation, three emitters still kept DR emission locations of 665–668 nm with good PLQYs (Figure S15, Supporting Information). Where, the fluorescence efficiency of TNZPPI was estimated about 38%, and was higher than common NZ-derivatives, implying our asymmetric modification and the introduction of PPI could effectively improve the luminescence efficiency in aggregates. While in TNZtPPI, its QY decreased to 24%, which might be due to the increase of the CT state ratio giving higher negative effect on its emitting

efficiency higher than the positive effect via inhibiting of molecular packing from tert-butyl group. When the inhibition from steric effect was further enhanced in TNZ2tPPI, the PLQY in film increased to 35% than single tert-butyl substitution, but it was still lower than TNZPPI. This phenomenon showed the electron effect at unimolecular level (LE and CT ratio distribution) became a more important factor in there, as well as inhibiting intermolecular interactions. The rational design of electron effect and inhibited intermolecular interaction ensured these luminescence efficiencies in solid state at a high level in the field of DR emitters.^[30–32]

The investigation about the change trend of luminescent behaviors under molecules aggregation process was also carried out. When water as poor solvent was added to DMF solution contained fluorophore with different proportion, the TNZPs would gradually aggregate into nanoparticles originating from hydrophobic interaction, and their PL emission intensity were obviously enhanced when water fraction (f_w) arrived to 40% as show in Figure 5, indicative of their AIE activity (Figure S16, Supporting Information). In comparison, the improvement ratio of TNZtPPI and TNZ2tPPI changed obviously with about 25 and 60 times, but in TNZPPI, the change was only 3 times. That is why? In fact, comparing their dipole moment at ground state and CT component ratio at excited state, TNZtPPI and TNZ2tPPI had higher CT component according to the above-mentioned Lippert–Mataga results, which usually was more sensitive to external polarity, similar to solvation effect above. When molecular aggregated into nanoparticles or films, the external higher-polarity DMF solvent field was replaced by the moderate polarity field provided by adjacent emitting molecules, and the enhanced intensity in their emission should be predicted. Combining with the calculation of the radiative decay rate (K_r) and the nonradiative decay rate (K_{nr}) in solution and film state (Table 1), the restriction of intermolecular motion mechanism also gave some contribution for their AIE behavior,^[33] especially in TNZtPPI and TNZ2tPPI, whose K_{nr} decreased obviously. Based on the above information, the AIE activity of TNZPs was mainly due to environmental polar changes, in addition to molecular accumulation factors. In comparison, TNZPPI and TNZ2tPPI had

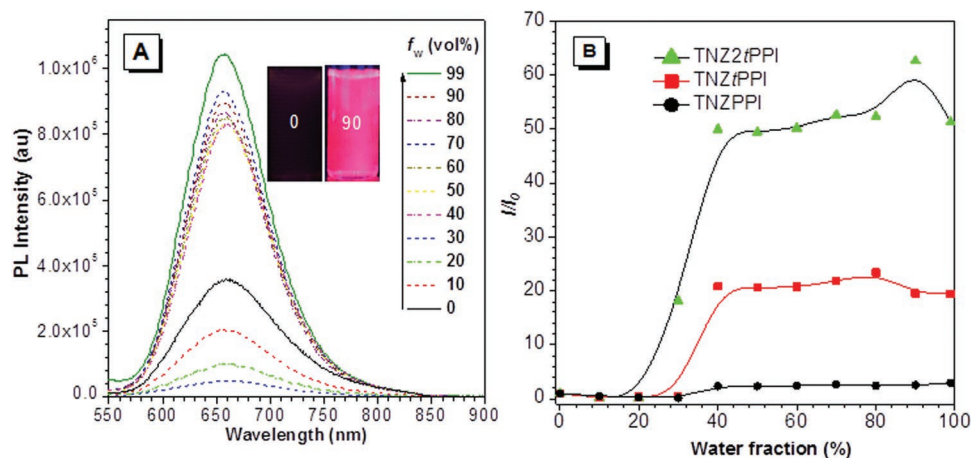


Figure 5. A) PL spectra of TNZPPI in DMF/water mixtures with different water fractions. B) Plot of I/I_0 (emission intensity)/ I_0 (emission intensity in DMF solvent) of TNZPs versus water fraction of the mixtures.

Table 1. The photophysical data of TNZPPI, TNZtPPI, and TNZ2tPPI.

Compounds	$\lambda_{\text{abs}}^{\text{a)}$ [nm]	$\lambda_{\text{em}}^{\text{b)}$ [nm]		$\Phi_{\text{r}}^{\text{c)}$ [%]		$\tau^{\text{d)}$ [ns]		$K_{\text{r}}^{\text{e)}$ [10^7 s^{-1}]		$K_{\text{nr}}^{\text{f)}$ [10^7 s^{-1}]	
	Soln	Soln	Film	Soln	Film	Soln	Film	Soln	Film	Soln	Film
TNZPPI	311/506	662	668	2.2	38	10.96	4.25	0.20	8.94	8.92	14.59
TNZtPPI	311/506	686	665	4.1	24	1.50	3.11	2.73	7.72	63.93	24.44
TNZ2tPPI	311/506	685	667	3.3	35	3.50	4.05	0.94	8.64	27.63	16.05

^{a)}Absorption peaks, concentration: 10^{-5} M ; ^{b)}Maximum emission wavelength, solution (Soln): DMF, concentration 10^{-5} M , Film: neat film with 80 nm; ^{c)}Absolute PLQY measured using an integrating sphere; ^{d)}Fluorescence lifetime; ^{e)} $K_{\text{r}} = \Phi_{\text{r}}/\tau$; ^{f)} $K_{\text{nr}} = (1-\Phi_{\text{r}})/\tau$.

showed similar excellent comprehensive performance with good luminescence efficiency, but the modification of tert-butyl group was of great significance to the study of structure–properties relationship, and the influence of reduced intermolecular packing interaction to the OLED performance would be clear for NZ-based materials.

For fabricating into OLED devices with good performance, three TNZPs' thermal properties were measured by thermogravimetric analysis and differential scanning calorimetry under nitrogen atmosphere (Figure S17, Supporting Information). They all exhibited good thermal stability with decomposition temperature of more than 250 °C. And the TNZPPI and TNZ2tPPI showed higher glass transition temperature (T_{g}) of 110 and 156 °C, and no obvious glass transition temperature was measured for TNZtPPI, suggesting their good morphological stability.

The electrochemical properties of emitters were measured by cyclic voltammetry in the CH_2Cl_2 and DMF solution containing 0.1 M tetra-*n*-butylammonium hexafluorophosphate. As shown in Figure S18 (Supporting Information), three TNZPs showed similar oxidation and reduction process. TNZtPPI and TNZ2tPPI possessed same HOMO energy level (−5.41 eV), and this value was lower than TNZPPI (−5.24 eV). The same situation was occurred at the LUMO levels, and the TNZtPPI and TNZ2tPPI located at −3.40 eV, while improved slightly to −3.22 eV in TNZPPI. The result showed that the former two had more similarities, while the latter was different, which was consistent to the electron distribution in the calculation above. However, the electrochemical energy gaps of TNZPs were very close, about 2.01–2.05 eV, which was similar to the optical energy gaps (2.09–2.11 eV) calculated from absorption spectra, suggesting the consistency of optical and electrochemical band gap. Additionally, three TNZPs emitters showed excellent reversibility of oxidation and reduction procedure, suggesting that great electrochemical stability during the charge injection and transport in OLED devices.

Thanks to their satisfying PLQYs in solid, better thermal and electrochemical properties, the undoped OLEDs based on three pure organic DR/NIR emitters were fabricated with multilayer devices structure: ITO/HATCN (5 nm)/TAPC (60 nm)/emitter (20 nm)/TmPyPB (50 nm)/LiF (1 nm)/Al (120 nm) (Emitter = TNZPPI or TNZtPPI or TNZ2tPPI). 1,4,5,8,9,11-hexaaza-triphenylene-hexacarbonitrile (HATCN) and LiF were used as the hole- and electron-injection materials, and 1,1'-Bis(di-4-tolylaminophenyl)cyclohexane (TAPC) was served as hole-transporting and exciton-blocking layers, and the 1,3,5-tri(m-pyrid-3-yl-phenyl)benzene (TmPyPB) was used as electron-transporting material (Figure 6A). The device results were summarized in Table 2.

The EL peaks of TNZPs were located at 678–686 nm (Figure S20, Supporting Information), and their CIE coordinates were located at (0.69, 0.30) or (0.69, 0.31), indicating their NIR emission behaviors in film have been well maintained in devices. All devices turned on at a low voltage of 2.9 eV, which was lower than common NIR-OLED devices,^[16,18,34] implying the fabricated device structure had lower carrier injection barrier. Additionally, the TNZPs-based devices possessed higher maximum red luminance of 1344–1938 cd m^{-2} , demonstrating efficient injection, transport and recombination of holes and electrons (Figure 6C). Encouragingly, three TNZPs emitters all showed higher maximum radiance of 21 447–36 027 $\text{mW Sr}^{-1} \text{ m}^{-2}$, which was higher than most reported pure organic NIR devices reported up to now, demonstrating the instruction of PPI group was very meaningful to increase brightness.^[12,35,36] All nondoped devices showed desirable efficiency, and TNZPPI-based device was superior to other two with maximal EQE of 2.48% (Table 2). Furthermore, TNZPPI exhibited very excellent comprehensive performance with PLQY of 38% in film, EQE of 2.48%@CIE (0.69, 0.30) and higher radiance of 36 027 $\text{mW Sr}^{-1} \text{ m}^{-2}$, which mainly originated from its special excited states distribution and composition, such as high ratio LE component in S_1 and effective triplet–singlet conversion at upper energy level.^[12,16,18,35–40]

Based on the analysis of their efficiencies in film and aggregation process, the interaction between luminescent molecules had a significant effect on efficiency. So, the doped devices were employed, and their structure with different doping concentration were carried out as ITO/HATCN (5 nm)/TAPC (60 nm)/CBP:emitters/TmPyPB (50 nm)/LiF (1 nm)/Al (120 nm), where emitters were composed of CBP host and the dopant of TNZPs was 5, 10, or 20 wt%. The performances of these doped devices were clearly listed in Table 2 (device D–L), and their PLQYs in doped film were listed in Table S4 (Supporting Information). While their corresponding EL spectra, curve of EQE versus brightness and current density–voltage–luminance (J – V – L) characteristics were provided in Figure S19 (Supporting Information). Comparing to nondoped devices, all of doped OLEDs displayed the enhanced EQEs. Especially, at doping concentration of 10 wt%, TNZPPI-based device with highest EQE of 6.83% exhibited excellent red color with CIE coordination of (0.67, 0.33), which was consistent to SSRL standard from NTSC.

In addition, some more detailed information about aggregation could be obtained from these doped devices. At doping concentration of 5 wt%, the luminescent molecules could be blocked by host materials, and their EQEs (6.56% for TNZPPI, 6.52% for TNZtPPI, and 4.66% for TNZ2tPPI) had the same change trend as their efficiencies in low-polarity solution (89.7% for TNZPPI, 82.9% for TNZtPPI, and 79.4% for TNZ2tPPI in

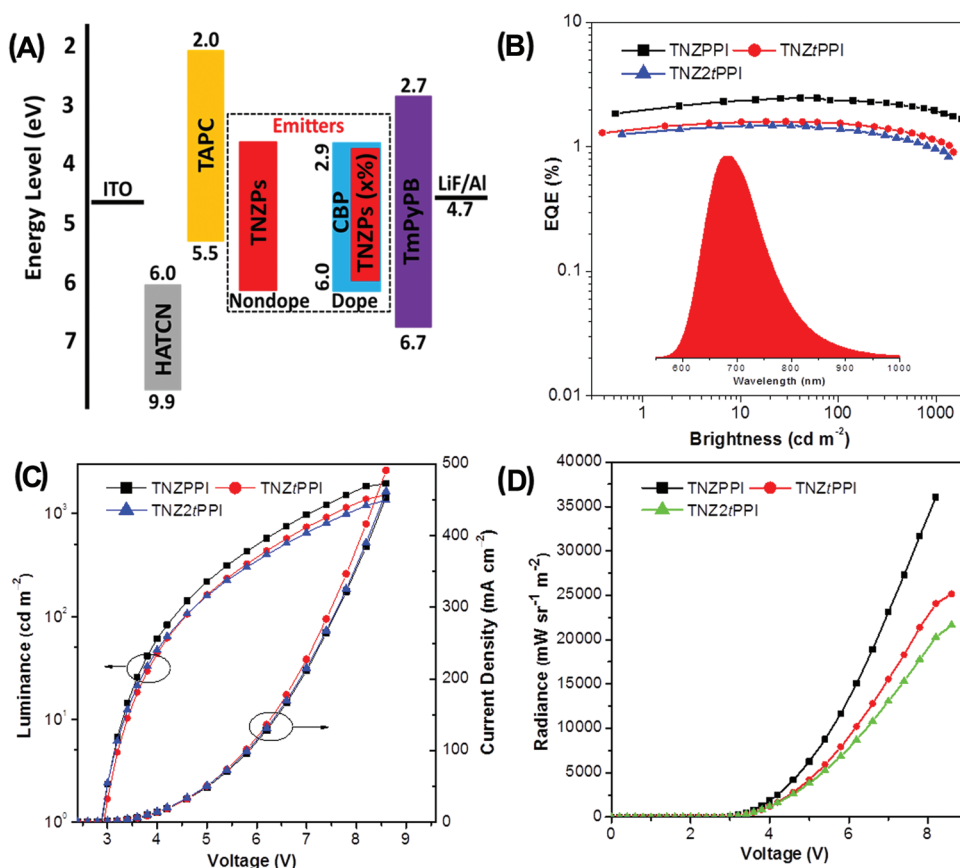


Figure 6. A) Diagram of the used materials in the devices. B) Curve of EQE versus brightness of devices. Inset: EL spectra of TNZPPi, TNZtPPI, and TNZ2tPPI. C) Current density–voltage–luminance (J – V – L) characteristics. D) Maximum radiance of TNZPPi, TNZtPPI, and TNZ2tPPI.

hexane), indicating that their excited states were less affected by the polarity field generated from other adjacent dopant's CT states. While at doping concentration of 10 wt%, the distance

between the guest luminescent molecules became narrower, and the interference between the lower CT component molecules (TNZPPi) was not obvious, its EQE was enhanced with

Table 2. EL performances of undoped and doped OLED devices.

Devices	λ_{EL} [nm]	V_{on}^a [V]	L^b [cd m $^{-2}$]	R^c [mW Sr $^{-1}$ m $^{-2}$]	η_c^d [cd A $^{-1}$]	η_p^e [lm W $^{-1}$]	EQE f [%]	FWHM g [nm]	CIE(x, y) h
A	686	2.9	1938	36 027	0.40	0.47	2.48	123	(0.69, 0.30)
B	686	2.9	1514	25 131	0.30	0.33	1.60	122	(0.69, 0.31)
C	678	2.9	1344	21 447	0.31	0.32	1.48	124	(0.69, 0.31)
D	642	3.5	2294	15 982	4.50	3.88	6.56	109	(0.64, 0.35)
E	642	3.7	2033	14 099	4.01	3.31	6.52	111	(0.64, 0.35)
F	642	3.7	1922	13 913	2.44	1.95	4.66	113	(0.65, 0.35)
G	648	3.7	2296	19 623	3.45	2.63	6.83	109	(0.67, 0.33)
H	654	3.7	699	6266	1.93	1.58	4.21	112	(0.67, 0.33)
I	654	3.7	1675	14 138	1.94	1.59	4.83	114	(0.67, 0.33)
J	666	3.1	2230	25 566	1.67	1.64	5.18	114	(0.67, 0.32)
K	660	3.3	1558	16 019	1.11	1.03	3.34	115	(0.67, 0.32)
L	664	3.1	1678	17 854	0.91	0.88	2.78	116	(0.67, 0.32)

^a) V_{on} is the turn-on voltage at 1 cd m $^{-2}$; ^b) The luminescence (L); ^c) Maximum radiance (R); ^d) Current efficiency (η_c); ^e) Power efficiency (η_p); ^f) Maximal external quantum efficiency; ^g) Full width at half maximum (FWHM); ^h) CIE coordinates at 10 mA cm $^{-2}$. Device configuration: ITO/HATCN (5 nm)/TAPC (60 nm)/emitter (20 nm)/TmPyPB (50 nm)/LiF (1 nm)/Al (120 nm). Emitters: TNZPPi (A); TNZtPPI (B); TNZ2tPPI (C); CBP: TNZPPi (5 wt%) (D); CBP: TNZtPPI (5 wt%) (E); CBP: TNZ2tPPI (5 wt%) (F); CBP: TNZPPi (10 wt%) (G); CBP: TNZtPPI (10 wt%) (H); CBP: TNZ2tPPI (10 wt%) (I); CBP: TNZPPi (20 wt%) (J); CBP: TNZtPPI (20 wt%) (K); CBP: TNZ2tPPI (20 wt%) (L).

the dopant ratio increase. While to the higher component CT molecules (TNZ*t*PPI), the interference between luminescent molecules became very significant, and its EQE of Device H gave a significant decline. In TNZ2*t*PPI, the EQE improvement of Device I was possibly due to its PLQY increment (47% in doped film) from the action of tert-butyl group. Lastly, at doping concentration of 20 wt%, the interaction between excited states of luminescent molecules was unavoidable, and their EQEs decreased as a whole, similar to nondoped system, but their performances were much better than that of devices in nondoped system. The detail results showed that, the doping process was an effective strategy to obtain better device performance for materials with more CT components in its excited state of luminescent molecules, which could limit the undesirable interference between dopants. In fact, three emitters all exhibited uniform color coordinates at the same concentration, demonstrating the introduction of tert-butyl group did not affect the band gap of luminescent core, and all emission was very stable and located at very valuable DR region with perfect higher radiance, which was very valuable for practical application in DR OLEDs construction. The recent research progress about DR/NIR devices using HLCT-AIE fluorophores as emitting layer is listed in Table S5 (Supporting Information), we can notice TNZP-based devices shows desirable device efficiency in both of nondoped/doped OLED devices.

To verify the predicted higher EUE from previous NTOs calculation, we estimated the practical excitons utilization ratio (η_r) according to the equation ($\text{EQE} = (\gamma \times \eta_r \times \phi_{\text{PL}}) \times \eta_{\text{out}}$). Where γ was the excitons recombination efficiency, usually served as 100%; ϕ_{PL} was the fluorescent quantum yield of emitters in neat film; η_{out} represented for the light out-coupling efficiency, regarded as 20% for the ITO glass substrate. For the most devices, we could consider that excitons achieved ideal recombination ($\gamma = 100\%$), the η_r of TNZPPI and TNZ*t*PPI were respectively thereby calculated as 33% and 34% in the nondoped devices. However, the η_r of three emitters enhanced to 82% (TNZPPI), 62% (TNZ*t*PPI), and 51% (TNZ2*t*PPI) in the doped devices with 10 wt% doped concentration. The enhanced EUE in the doped system suggests that doped method not only avoids fluorescence quenching, but also weaken interaction between excitons. Importantly, the EUEs in the doped/nondoped devices surpassed the 25% upper limitation of conventional common fluorophores, demonstrating efficient “hot exciton” channel to improve the triplet excitons harvesting, which were well matched with theoretical simulation.

3. Conclusion

In summary, three new NIR luminogens based on TPA-modified NZ-framework were prepared after inserting a planar group of PPI as asymmetric substitution group, and the different pattern tert-butyl groups in PPI were also introduced to tuning intermolecular interaction between emitters. Employing quantum chemical calculations, their hybrid excited states of LE and CT components were confirmed, and the effective uRISC channel might be activated because of their larger T_2 – T_1 energy gap as well as smaller T_4 – S_2 energy splitting, which could lead to the efficient triplet excitons conversion channel

and be benefitted to enhance EUE in OLED operation. Thanks for systematic photophysical characterizations, their special excited state components changes were discussed deeply, and the emitters became more sensitive to external environmental polarity after inserting larger steric hindrance groups. Luckily, these new comers exhibited good NIR emission in film with higher PLQYs than common NZ-based derivatives, and enjoyed AIE activity when aggregating to nanoparticles from DMF solution. The efficiency of TNZPPI in film could reach to 38%, and its nondoped device realized higher EQE of 2.48% @ CIE (0.69, 0.30) and higher radiance of 36 027 mW Sr^{−1} m^{−2}, whose comprehensive performance were obviously better than most reported NIR materials. Excitingly, TNZPs-based doped OLEDs with CBP as host exhibit excellent performance with identical NTSC saturated red-emitters standard, and enjoying higher EUEs for uRISC activated. Combining with a series of analysis, the structure–properties relationship of TPA modified NZ-based emitters become clear, the role of intramolecular electronic effect of molecule structure and intermolecular stacking interactions all were relative to their performance in TNZPs-based materials, which was very important to design high-efficiency NZ-based DR/NIR fluorescent OLED materials.

Supporting Information

Supporting Information is available from the Wiley Online Library or from the author.

Acknowledgements

Q.W. and J.T. contributed equally to this work. The authors are grateful for financial support from the National Natural Science Foundation of China (21788102, 51673118, and 21975077), Natural Science Fund of Guangdong Province (2016A030312002), Innovation and Technology Commission of Hong Kong (ITC-CNERC14SC01), Science & Technology Program of Guangzhou (201804020027, 201804010218, and 201704030069), Fundamental Research Funds for the Central Universities (2019ZD04), and Fund of Key Laboratory of Luminescence from Molecular Aggregates of Guangdong Province (2019B030301003).

Conflict of Interest

The authors declare no conflict of interest.

Keywords

aggregation-induced emission, higher radiance, hybrid excited states, organic light emitting diodes, saturated red-emitting light

Received: September 6, 2019

Revised: November 6, 2019

Published online: December 18, 2019

[1] X. Yang, G. Zhou, W. Y. Wong, *Chem. Soc. Rev.* **2015**, *44*, 8484.

[2] Q. Zhang, B. Li, S. Huang, H. Nomura, H. Tanaka, C. Adachi, *Nat. Photonics* **2014**, *8*, 326.

- [3] D. Zhang, L. Duan, C. Li, Y. Li, H. Li, D. Zhang, Y. Qiu, *Adv. Mater.* **2014**, 26, 5050.
- [4] Y. Qu, M. Slootsky, S. R. Forrest, *Nat. Photonics* **2015**, 9, 758.
- [5] K. Udagawa, H. Sasabe, C. Cai, J. Kido, *Adv. Mater.* **2014**, 26, 5062.
- [6] A. Shao, Y. Xie, S. Zhu, Z. Guo, S. Zhu, J. Guo, P. Shi, T. D. James, H. Tian, W. H. Zhu, *Angew. Chem.* **2015**, 127, 7383.
- [7] J. Liu, K. Li, B. Liu, *Adv. Sci.* **2015**, 2, 1500008.
- [8] M. Kang, X. Gu, R. T. K. Kwok, C. W. T. Leung, J. W. Y. Lam, F. Li, B. Z. Tang, *Chem. Commun.* **2016**, 52, 5957.
- [9] Y. Pan, W. Li, S. Zhang, L. Yao, C. Gu, H. Xu, B. Yang, Y. Ma, *Adv. Opt. Mater.* **2014**, 2, 510.
- [10] V. Jankus, C. J. Chiang, F. Dias, A. P. Monkman, *Adv. Mater.* **2013**, 25, 1455.
- [11] J. V. Caspar, E. M. Kober, B. P. Sullivan, T. J. Meyer, *J. Am. Chem. Soc.* **1982**, 104, 630.
- [12] J. Xue, C. Li, L. Xin, L. Duan, J. Qiao, *Chem. Sci.* **2016**, 7, 2888.
- [13] W. Li, Y. Pan, R. Xiao, Q. Peng, S. Zhang, D. Ma, F. Li, F. Shen, Y. Wang, B. Yang, Y. Ma, *Adv. Funct. Mater.* **2014**, 24, 1609.
- [14] T. Liu, G. Xie, C. Zhong, S. Gong, C. Yang, *Adv. Funct. Mater.* **2018**, 28, 1706088.
- [15] T. Liu, L. Zhu, S. Gong, C. Zhong, G. Xie, E. Mao, J. Fang, D. Ma, C. Yang, *Adv. Opt. Mater.* **2017**, 5, 1700145.
- [16] T. Liu, L. Zhu, C. Zhong, G. Xie, S. Gong, J. Fang, D. Ma, C. Yang, *Adv. Funct. Mater.* **2017**, 27, 1606384.
- [17] C. Wang, X. L. Li, Y. Gao, L. Wang, S. Zhang, L. Zhao, P. Lu, B. Yang, S. J. Su, Y. Ma, *Adv. Opt. Mater.* **2017**, 5, 1700441.
- [18] X. Tang, X. L. Li, H. Liu, Y. Gao, Y. Shen, S. Zhang, P. Lu, B. Yang, S. J. Su, Y. Ma, *Dyes Pigm.* **2018**, 149, 430.
- [19] H. Zhang, J. Zeng, W. Luo, H. Wu, C. Zeng, K. Zhang, W. Feng, Z. Wang, Z. Zhao, B. Z. Tang, *J. Mater. Chem. C* **2019**, 7, 6359.
- [20] S. Zhang, L. Yao, Q. Peng, W. Li, Y. Pan, R. Xiao, Y. Gao, C. Gu, Z. Wang, P. Lu, F. Li, S. Su, B. Yang, Y. Ma, *Adv. Funct. Mater.* **2015**, 25, 1755.
- [21] X. Tang, T. Shan, Q. Bai, H. Ma, X. He, P. Lu, *Chem. - Asian J.* **2017**, 12, 552.
- [22] Q. Wan, B. Zhang, J. Tong, Y. Li, H. Wu, H. Zhang, Z. Wang, Y. Pan, B. Z. Tang, *Phys. Chem. Chem. Phys.* **2019**, 21, 9837.
- [23] W. Li, D. Liu, F. Shen, D. Ma, Z. Wang, T. Feng, Y. Xu, B. Yang, Y. Ma, *Adv. Funct. Mater.* **2012**, 22, 2797.
- [24] T. Northey, T. Keane, J. Eng, T. J. Penfold, *Faraday Discuss.* **2019**, 216, 395.
- [25] M. K. Etherington, J. Gibson, H. F. Higginbotham, T. J. Penfold, A. P. Monkman, *Nat. Commun.* **2016**, 7, 13680.
- [26] X. K. Chen, S. F. Zhang, J. X. Fan, A. M. Ren, *J. Phys. Chem. C* **2015**, 119, 9728.
- [27] J. Gibson, A. P. Monkman, T. J. Penfold, *ChemPhysChem* **2016**, 17, 2956.
- [28] Y. Gao, S. Zhang, Y. Pan, L. Yao, H. Liu, Y. Guo, Q. Gu, B. Yang, Y. Ma, *Phys. Chem. Chem. Phys.* **2016**, 18, 24176.
- [29] S. Zhang, W. Li, L. Yao, Y. Pan, F. Shen, R. Xiao, B. Yang, Y. Ma, *Chem. Commun.* **2013**, 49, 11302.
- [30] A. Nicol, W. Qin, R. T. K. Kwok, J. M. Burkhartsmeier, Z. Zhu, H. Su, W. Luo, J. W. Y. Lam, J. Qian, K. S. Wong, B. Z. Tang, *Chem. Sci.* **2017**, 8, 4634.
- [31] F. Zhang, Y. Di, Y. Li, Q. Qi, J. Qian, X. Fu, B. Xu, W. Tian, *Dyes Pigm.* **2017**, 142, 491.
- [32] Z. Zheng, T. Zhang, H. Liu, Y. Chen, R. T. K. Kwok, C. Ma, P. Zhang, H. H. Y. Sung, I. D. Williams, J. W. Y. Lam, K. S. Wong, B. Z. Tang, *ACS Nano* **2018**, 12, 8145.
- [33] N. L. C. Leung, N. Xie, W. Yuan, Y. Liu, Q. Wu, Q. Peng, Q. Miao, J. W. Y. Lam, B. Z. Tang, *Chem. - Eur. J.* **2014**, 20, 15349.
- [34] C. Li, R. Duan, B. Liang, G. Han, S. Wang, K. Ye, Y. Liu, Y. Yi, Y. Wang, *Angew. Chem., Int. Ed.* **2017**, 56, 11525.
- [35] W. W. H. Lee, Z. Zhao, Y. Cai, Z. Xu, Y. Yu, Y. Xiong, R. T. K. Kwok, Y. Chen, N. L. C. Leung, D. Ma, J. W. Y. Lam, A. Qin, B. Z. Tang, *Chem. Sci.* **2018**, 9, 6118.
- [36] X. Du, J. Qi, Z. Zhang, D. Ma, Z. Y. Wang, *Chem. Mater.* **2012**, 24, 2178.
- [37] M. Shimizu, R. Kaki, Y. Takeda, T. Hiayama, N. Nagai, H. Yamagishi, H. Furutani, *Angew. Chem.* **2012**, 124, 4171.
- [38] X. Han, Q. Bai, L. Yao, H. Liu, Y. Gao, J. Li, L. Liu, Y. Liu, X. Li, P. Lu, B. Yang, *Adv. Funct. Mater.* **2015**, 25, 7521.
- [39] L. Yao, S. Zhang, R. Wang, W. Li, F. Shen, B. Yang, Y. Ma, *Angew. Chem., Int. Ed.* **2014**, 53, 2119.
- [40] A. Obolda, X. Ai, M. Zhang, F. Li, *ACS Appl. Mater. Interfaces* **2016**, 8, 35472.